Delft University of Technology

Masters in Systems and Control

Robust Control Assignment

Part 2

December 18, 2020

Contents

List of Figures

1 Motivation

In Part 1 of the assignment we saw that the SISO design generally provides poor settling time for reference tracking. Moreover, the designed controller was not applicable for both reference tracking and disturbance rejection. The generator torque input was not used for the control.

By implementing multivariable mixed-sensitivity design the performance and disturbance rejection properties can be improved. In this part of the assignment we use H_∞ controller synthesis with weights, using the Robust Control Toolbox in MATLAB.

For control both controllable inputs are used (β pitch angle, τ generator torque). In Section 2 the main goal is to design a reference tracking controller. There the effect of the disturbance channel is not considered explicitly for the controller synthesis.

In Section 3 the transfer function of the wind disturbance is also considered. There the main objective is to design a disturbance rejection controller for a given operating point. Also there we want to make a distinction that the β control input operates on lower frequencies and the τ on higher frequencies.

2 Multivariable mixed-sensitivity design

For this part of the project, the inputs of the plant are the pitch angle and the generator torque, while its outputs are the turbine rotational speed and the wind turbine fore-aft displacement. This implies that the system is now multiple-input multiple-output (MIMO), which brings larger design capabilities, as will be discussed along this document.

As a new requirement, it is desired to keep the static power curve of the generator torque unchanged, meaning that the torque control input is not allowed to have a steady-state contribution.

2.1 Relative gain array calculation

The relative gain array (RGA) is a frequency-dependent representation of how each input of the plant individually affect each output. The RGA is defined in the following way:

$$\mathrm{RGA}(G) = G \times \left(G^{-1}\right)^T \tag{1}$$

The RGA numerical expression has been computed using Equation 1 in Matlab, both for $w = 0$ and $w = 0.4 * 2\pi$ $[rad/s]$, as hereafter shown:

$$RGA(0) = \begin{bmatrix} -0.6554 & 1.6554 \\ 1.6554 & -0.6554 \end{bmatrix} \tag{2}$$

$$RGA(0.4 \cdot 2\pi) = \begin{bmatrix} -0.0117 + 0.1068i & -0.9217 - 0.4306i \\ 0.9729 - 0.2973i & -0.0034 + 0.1074i \end{bmatrix} \tag{3}$$

It can be observed that for constant inputs ($w = 0$), there is a negative RGA between the pitch angle (first input) and the rotational speed (first output), as well as between the generator torque (second input) and the wind turbine fore-aft displacement (second output). Moreover, it can be remarked that the rotational speed is more influenced by the generator torque than by the pitch angle. Conversely, the effect of the pitch angle on the wind turbine displacement is larger than of the generator torque.

For high frequency inputs, the components of the RGA become complex, this is, a phase shift is introduced between the inputs and the outputs. Moreover, looking at the absolute value of the RGA's components (shown in Equation 4), it can be observed the difference between the inputs' influence on the outputs is enlarged.

This means that the generator torque affects the turbine's rotational speed more (1 order of magnitude) than the pitch angle. In the same way, the pitch angle has an impact on the wind

turbine displacement of 1 order of magnitude higher than the torque. For this reason, at high frequencies the plant is almost decoupled, and thus the rotational speed have to be controlled by the generator torque at those frequencies. This fact will affect the weight choices in the following sections.

$$RGA(0.4 \cdot 2\pi) = \begin{bmatrix} 0.1074 & 1.0173 \\ 1.0173 & 0.1074 \end{bmatrix} \tag{4}$$

As a final remark, it can be mentioned that for a $2x2$ matrix, the rows of the RGA shall add up to one, and its diagonal terms shall be equal, as well as the anti-diagonal ones. This is fulfilled by the $RGA(0)$, although the case for $RGA(0.4 \cdot 2\pi)$ can first seem not to fulfill it. Nevertheless, looking at 4 it can be observed that the diagonal and anti-diagonal terms are the same. In order to check that the row components add up to one, it shall be taken the absolute value of the row values added up in complex form.

2.2 Computation of the MIMO poles and zeros

In MIMO systems, it has to be taken into account that the zeros are the values which decrease the plant transfer function rank. Therefore, they can not be computed in the same way than for SISO systems. In this case, they have been calculated using the command *tzero* in Matlab.

For the wind turbine plant, the calculated zeros are the following:

$$z_1 = -0.0078 + 1.2358i \tag{5}$$
$$z_2 = -0.0078 - 1.2358i \tag{6}$$

There is substantial difference with the case of the SISO plant, which have right-half-plane (RHP) zeros, while in the MIMO case the RHP do not appear. Therefore, the RHP zeros represents a bandwidth limitation for the SISO case, but not for the MIMO.

In order to study the plant stability, the system poles are calculated:

$$p_1 = -0.0832 + 3.2936i \tag{7}$$
$$p_2 = -0.0832 - 3.2936i \tag{8}$$
$$p_3 = -0.0106 + 0.2022i \tag{9}$$
$$p_4 = -0.0106 - 0.2022i \tag{10}$$
$$p_5 = -0.4104 \tag{11}$$

It is shown that all the poles have negative real part, and thus the plant is stable. Moreover, it can be remarked that there is one real pole and two pairs of complex conjugate poles, which represent an oscillatory behaviour.

2.3 Output error weight design (W_{p11})

The weight W_{p11} represents the penalization on the sensitivity function of the pitch angle to the rotational speed.

From the provided weight data, a W_{p11} with the following structure can be designed:

$$W_{p11} = \frac{\frac{s}{M} + wb}{s + wb \cdot A} \tag{12}$$

The cut-off frequency of 0.4 can be translated to a w_b of $0.4 \cdot 2\pi$ $[rad/s]$, while the low-frequency disturbance attenuation requirement implies an A of 10^{-4}. Finally, the H_∞ norm of the sensitivity

function has to be 1.8, which can be directly related to an M term of 1.8.

$$W_{p11} = \frac{s + 4.524}{1.8s + 4.524 \cdot 10^{-4}} \tag{13}$$

2.4 Block diagram of the general design

Figure 1 shows the negative feedback block diagram for the model of the controlled floating wind turbine. For this part, the design will be performed for a model without disturbance and thus no disturbance input is taken into account.

The block diagram is composed by the weight for the error (W_p), the weight for the controller outputs (W_u), the state-space system with the pitch and torque as inputs and rotational speed and turbine displacement as outputs ($FWT(1:2, 1:2)$), and the controller (K).

The most relevant signals in the design are the reference input (w), the controller signal output (u), which coincides with the plant input, and the output error, or controller input signal (v). Finally, the outputs (Z_1) and (Z_2) show the weighted system's error and controller's output, respectively.

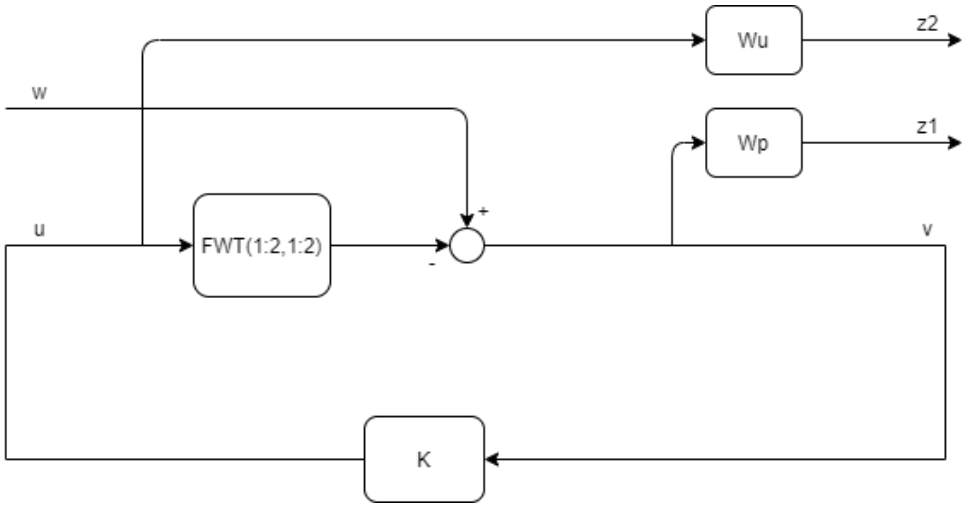

Figure 1: Block diagram with negative feedback

2.5 Generalized plant design and analysis

The generalized plant can be obtained by including the blocks inside the green area in Figure 2 into a common block P, as shown in Figure 3. Nevertheless, Figure 2 is useful to give a mathematical description of the new block diagram.

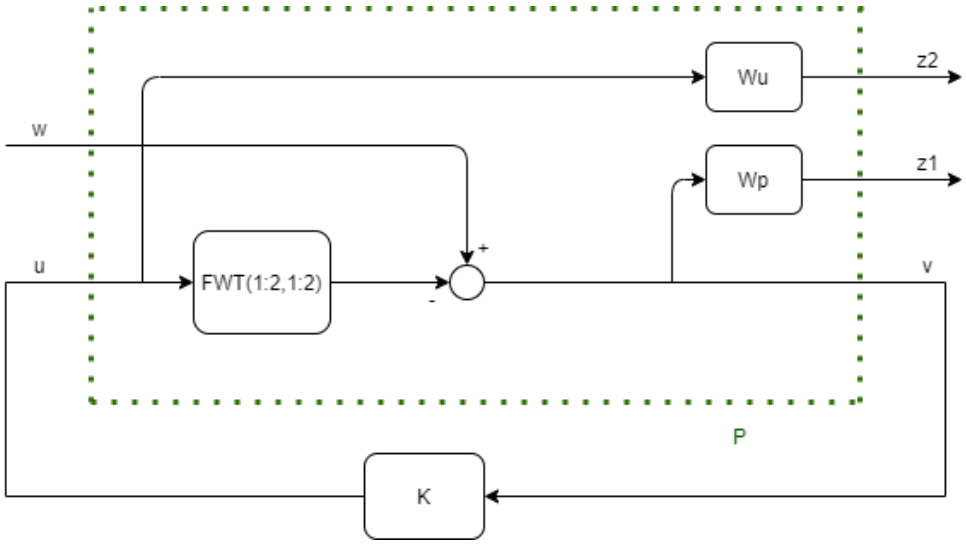

Figure 2: Block diagram for generalized plant with negative feedback

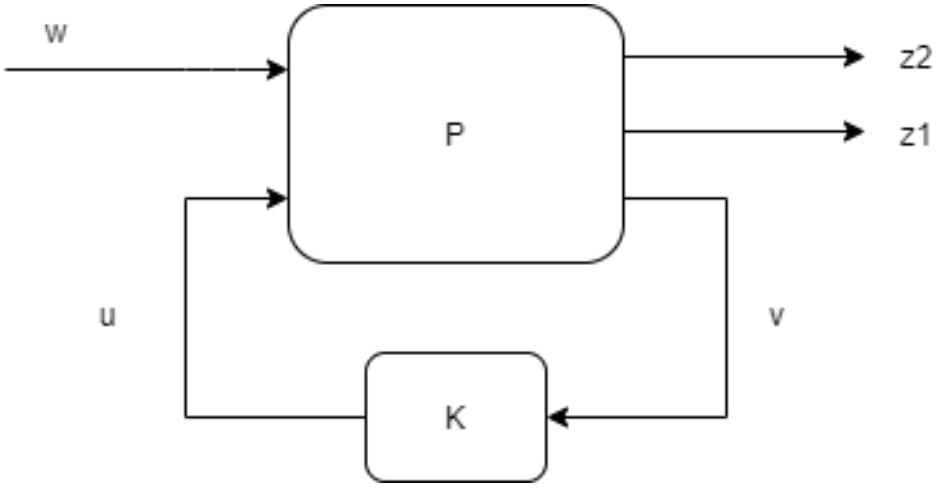

Figure 3: Generalized plant for reference tracking

The output $Z1$ is composed by the multiplication of the weight W_p and the system error, this is, the subtraction of the reference input w and the signal u multiplied by the modified plant. Moreover, the output $Z2$ is directly the input from the controller (u) multiplied by W_u, while the output signal v is the previously mentioned system error.

Taking into account these relationships, and referring to the state-space $FWT(1;2,1:2)$ as G for the shake of compactness, the mathematical description of the generalized plant can be derived:

$$\begin{bmatrix} z_1 \\ z_2 \\ v \end{bmatrix} = \underbrace{\begin{bmatrix} W_p & -W_pG \\ 0 & W_u \\ I & -G \end{bmatrix}}_{P} \begin{bmatrix} w \\ u \end{bmatrix} \tag{14}$$

Transforming G, W_p and W_u into state-space form, it can be observed that they have 5, 1 and 2 states, respectively. For this reason, it is expected that the generalized plant has 8 states. This has been verified using Matlab (bearing in mind to use the command *minreal* to the state-space system to avoid extra states).

2.6 Performance weights interpretation

The weight Wp, shown in Equation 15, represents the penalization on the rotational speed and wind turbine errors. It can be observed it is a diagonal matrix, this is, the errors are weighted independently. Therefore, Wp_{11} weights the rotational speed error. The Bode diagram of the weight, shown in Figure 4, gives relevant information on its purpose.

$$W_p = \begin{bmatrix} W_{p11} & 0 \\ 0 & 0.2 \end{bmatrix} \tag{15}$$

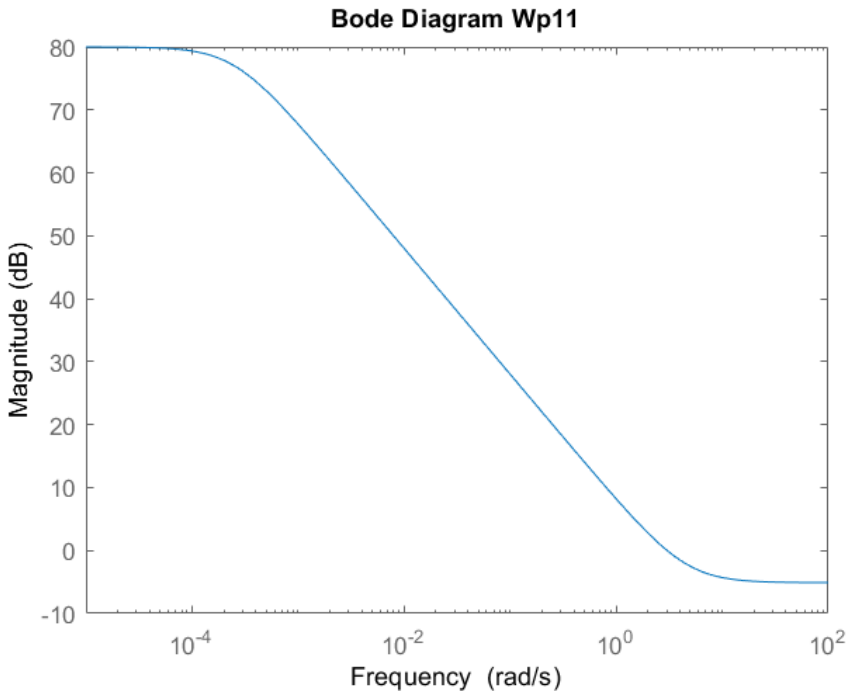

Figure 4: Bode diagram of Wp_{11}

Figure 4 shows that the weight highly penalizes the error at low frequencies, while the penalization for errors above 10 $[rad/s]$ is almost 0 dB. This is translated in the optimization problem as an influence to avoid the rotational speed to have steady-state error.

The term Wp_{22} is constant and relatively low in comparison to Wp_{11}, which means that the behaviour of the wind turbine displacement is not relevant in the optimization problem.

The weight W_u is shown in Equation 16, and, as in the previous case, it is a diagonal matrix. In this case, it represents the penalization on the controller outputs signal u, also referred to as control inputs.

$$W_u = \begin{bmatrix} 0.01 & 0 \\ 0 & Wu_{22} \end{bmatrix} \tag{16}$$

The weight W_{u11} is an small, constant term, which means that the beta control input is not penalized at any specific frequency, or in other words, the controller can actuate via the pitch angle at any frequency and with high gain (due to the low value of the weight).

In order to analyze the weight on the generator torque control input (Wu_{22}), its Bode diagram is shown in Figure 5. It can be highlighted that the weight mainly penalizes the response at low frequencies, while it allows large torque control action at frequencies above $0.01[rad/s]$.

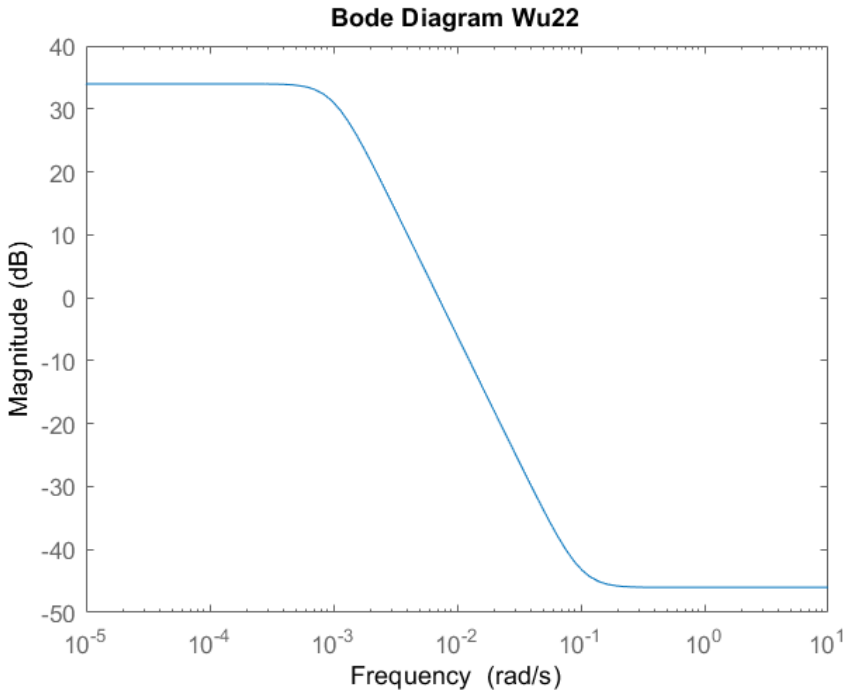

Figure 5: Bode diagram of Wu_{22}

This can be directly related to the desire of not having a steady-state contribution from the torque stated at the beginning of this document. Expressed in other words, the high penalty of the weight at low frequencies will force the controller to generate only high-frequency torque control inputs, and thus fulfill the zero steady-state requirement.

2.7 Mixed-sensitivity controller synthesis

The mathematical description of Equation 14 and the $hinfsyn$ Matlab command can be used to design the mixed-sensitivity generalized controller for P.

In order to address the system internal stability, one can refer to the stability of the system transfer function G and the transfer function Q, given:

$$Q = K(I + GK)^{-1} \tag{17}$$

where K is the controller obtained by the $hinfsyn$ command.

It can be shown that, if G is stable, then the system is internally stable if and only if Q is stable [1] . It shall be recall that the MIMO poles of G have been already calculated in Section 1.2, where it has been concluded that G is stable. Therefore, the closed-loop internal stability relies on the stability of Q.

In this analysis, the stability of Q will be proved by the Generalized Nyquist plot of the closed-loop system.

The Generalized Nyquist theorem [1] states that a closed-loop system is stable if and only if the Nyquist Plot of $det(I + L(s))$ makes P anti-clockwise encirclements of the origin and does

not cross the origin, where P is the number of unstable poles of the open-loop transfer function L(s).

The unstable poles of the open-loop transfer function $L(s)$ can be obtained by computing the poles of $G(s)K(s)$, which are the following:

$$p_1 = -34.0428 \tag{18}$$
$$p_2 = 0.0083 + 3.4260i \tag{19}$$
$$p_3 = 0.0083 - 3.4260i \tag{20}$$
$$p_4 = -0.0671 + 0.2130i \tag{21}$$
$$p_5 = -0.0671 - 0.2130i \tag{22}$$
$$p_6 = -0.0572 + 0.0637i \tag{23}$$
$$p_7 = -0.0572 - 0.0637i \tag{24}$$
$$p_8 = -0.0003 \tag{25}$$

where $p2$ and $p3$ are the RHP poles of $L(s)$.

The Generalized Nyquist Plot is shown in 6, and it can be observed that it encircles the origin two times in anti-clockwise direction (and it does not cross the origin). Therefore, it can be claimed that the closed-loop system is stable.

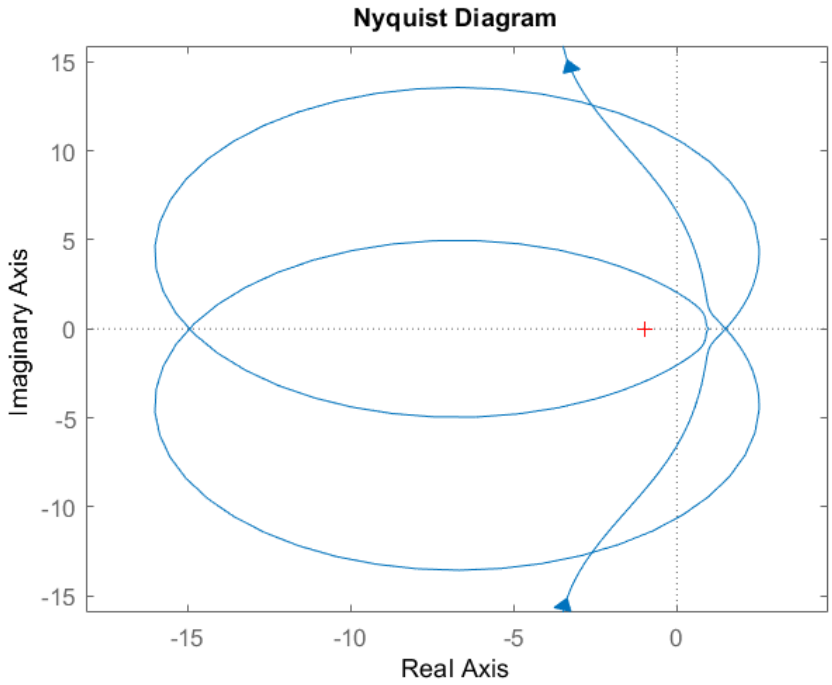

Figure 6: Nyquist diagram of $det(I + L(s))$

The closed-loop system has the following transfer function:

$$CL = GK(I + GK)^{-1} \tag{26}$$

It can be affirmed that, since it is stable, it does not have unstable poles. The fact that it does not have unstable poles can be due to two possibilities. The first one is that neither K, G or $(I + GK)^{-1}$ have unstable poles. The second one is that some of them have unstable poles but they are cancelled by some other's transfer function unstable zeros.

At this point, it is important to remember that G was proved not to have unstable zeros in Section 2.1. Therefore, the zeros from G can not cancel any RHP pole from K or $(I + GK)^{-1}$ and it can be concluded that neither $K(I + GK)^{-1}$ has unstable poles (could be because the individual functions do not have unstable poles or because there are unstable pole-zero cancellations).

Finally, realizing that $K(I + GK)^{-1}$ is exactly the expression for Q, it can be claimed that Q is stable, and thus the system is internally stable.

As a further analysis, it can be shown that indeed the controller K is unstable. Since G does not have either unstable poles or zeros, the unstable poles of K are exactly the $p2$ and $p3$ from $L(s)$ previously mentioned. Moreover, an unstable pole-zero cancellation happens between K and $(I + GK)^{-1}$, which makes Q stable.

It is expected that the number of states of the controller is the same than the generalized plant [1], which was proved to be eight. Again, using Matlab and the command *minreal* it has been confirmed that the controller has eight states.

2.8 Time-domain simulations

In order to perform the disturbance rejection simulations, the complete state-space system of the wind turbine has been used, although the controller K only influences the two first inputs (the pitch angle and the torque).

For the reference tracking simulation, a step input is introduced as reference for the rotational speed, which is shown in Figure 7. The system has a settling time of 10.4 $[s]$ and an overshoot of 6%. One can observe that the current settling time is eight times smaller than the settling time for the SISO case (which was 83.7$[s]$). Nevertheless, the overshoot is more than six times that of the SISO case.

It shall be remarked that the reference tracking of the wind turbine displacement (z) has not been simulated since it is understood it is not a control objective.

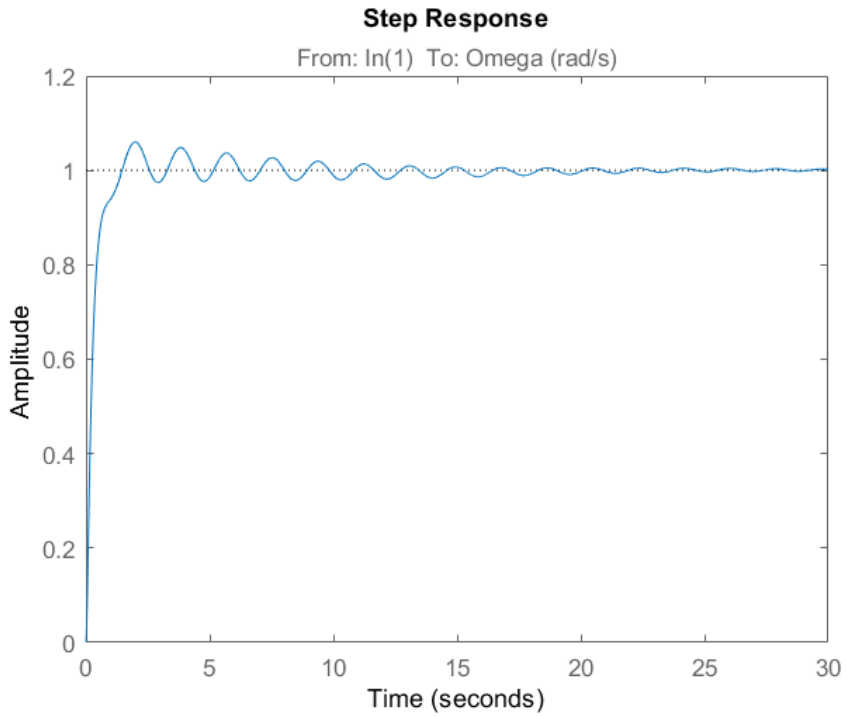

Figure 7: Reference tracking simulation

For the disturbance rejection simulation, a step input is introduced in the wind channel input. The system response, shown in Figure 8, has a settling time of 66.7 $[s]$, while for the SISO case it was 168 $[s]$, and a peak amplitude of 0.04, while that of the SISO system was 0.4.

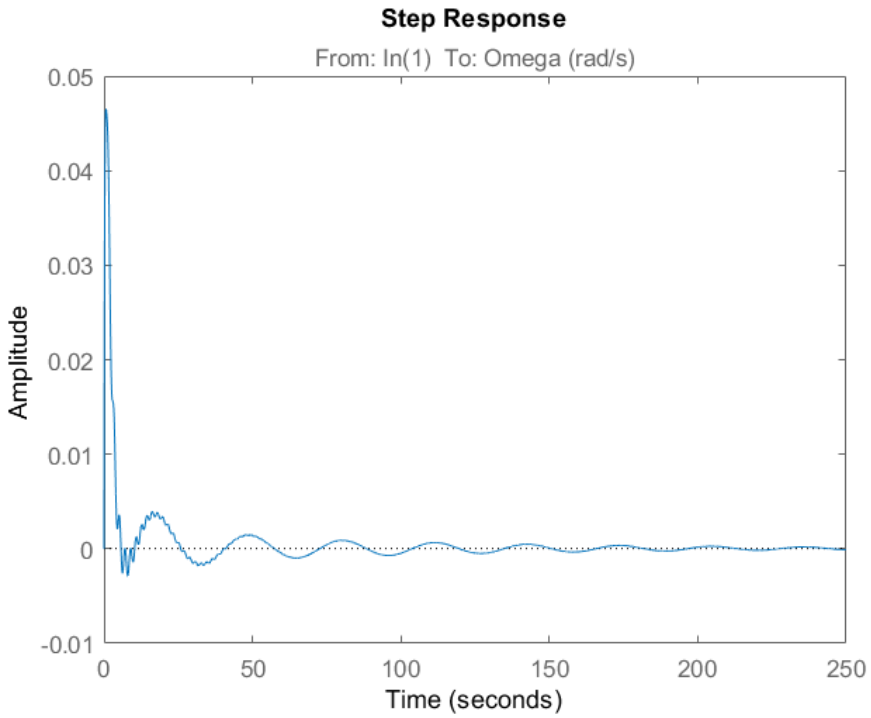

Figure 8: Disturbance rejection simulation

In order to achieve better performances, the weights can be adjusted. Nevertheless, this would imply a larger controller effort, which is limited by the wind turbine operational parameters of rated torque and speed.

3 MIMO disturbance rejection

3.1 Deriving the generalized plant

Figure 9 shows the block diagram of the generalized plant for this case with the controller. The input w now contains the disturbance input channel. The transfer function G_d is extracted from the state-space model of the wind turbine (FWT). It describes the connection between the disturbance input and the generator speed output. Also in this case we only consider the first output of the system for the H_∞ controller synthesis.

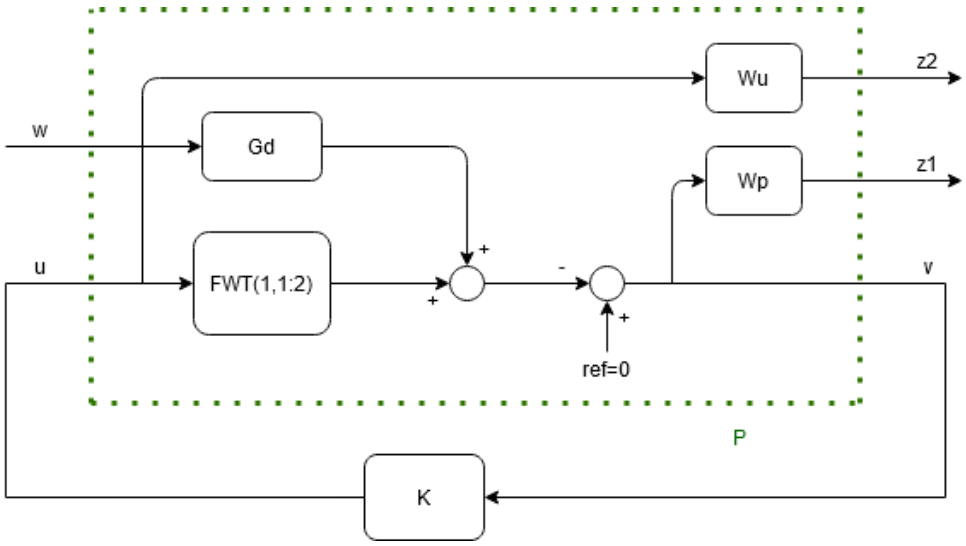

Figure 9: Block diagram of the generalized plant

The mathematical description of the generalized plant can be derived similarly to the previous part. So by looking at the paths from the outputs to the inputs we get the following expression:

$$\begin{bmatrix} z_1 \\ z_2 \\ v \end{bmatrix} = \underbrace{\begin{bmatrix} -W_p G_d & -W_p G \\ 0 & W_u \\ -G_d & -G \end{bmatrix}}_{P} \begin{bmatrix} w \\ u \end{bmatrix} \tag{27}$$

3.2 Designing the error weight

The first performance output z_1 in our case is the weighted system output (it is multiplied by -1 but for the synthesis only the amplitude matters). We want to suppress the influence of the disturbance input as much as possible and have values close to 0 in z_1, which result in values close to 0 in the ω output. That would mean that the generator is running close to the nominal frequency.

Relating this requirement to the Bode plot of the desired closed loop system: we want to have as small gain as possible for the complementary sensitivity function between the disturbance input and the ω output. A generally good disturbance rejection can be achieved if this Bode diagram curve is bellow $-20dB$ at all frequencies. The system bode plot for disturbance input and ω output is shown in Figure 10 together with the requirement.

Based on this frequency domain interpretation the weight can be determined. By the W_p weight we are limiting the bode magnitude curve of the following expression:

$$|W_p S G_d| < 1 \quad \rightarrow \quad |S G_d| < \frac{1}{W_p} \tag{28}$$

The system inherently suppressing disturbances at frequencies higher than $1[Hz]$. This means that it is sufficient to define a W_p weight which has high values on frequencies bellow $1[Hz]$. The designed weight is shown on Figure 11 .

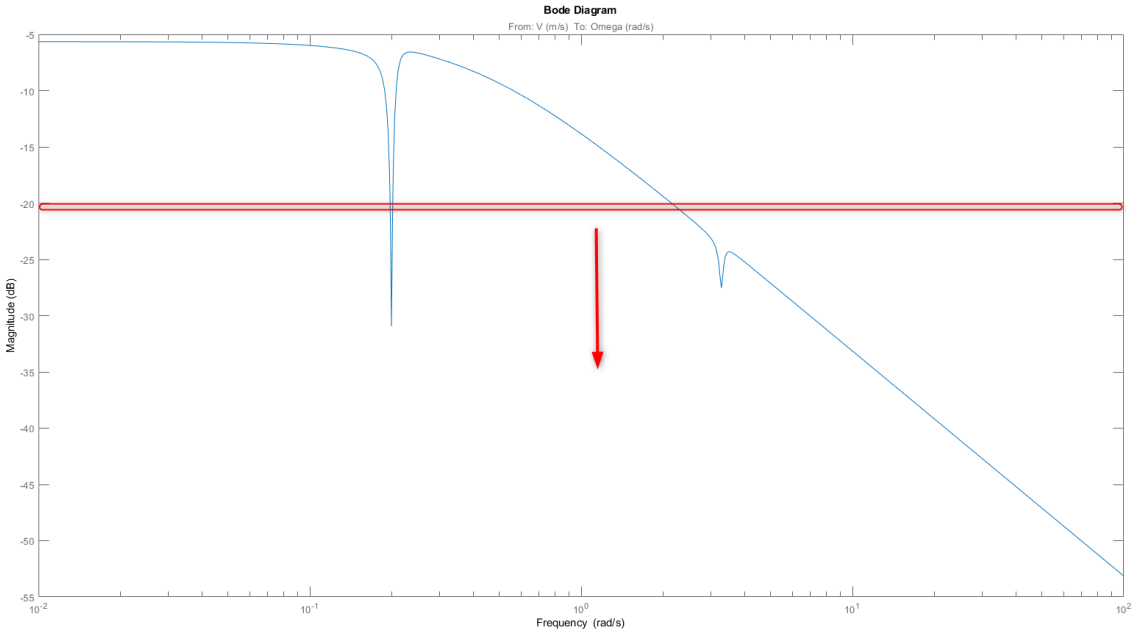

Figure 10: Bode diagram of G_d and the requirement for the design

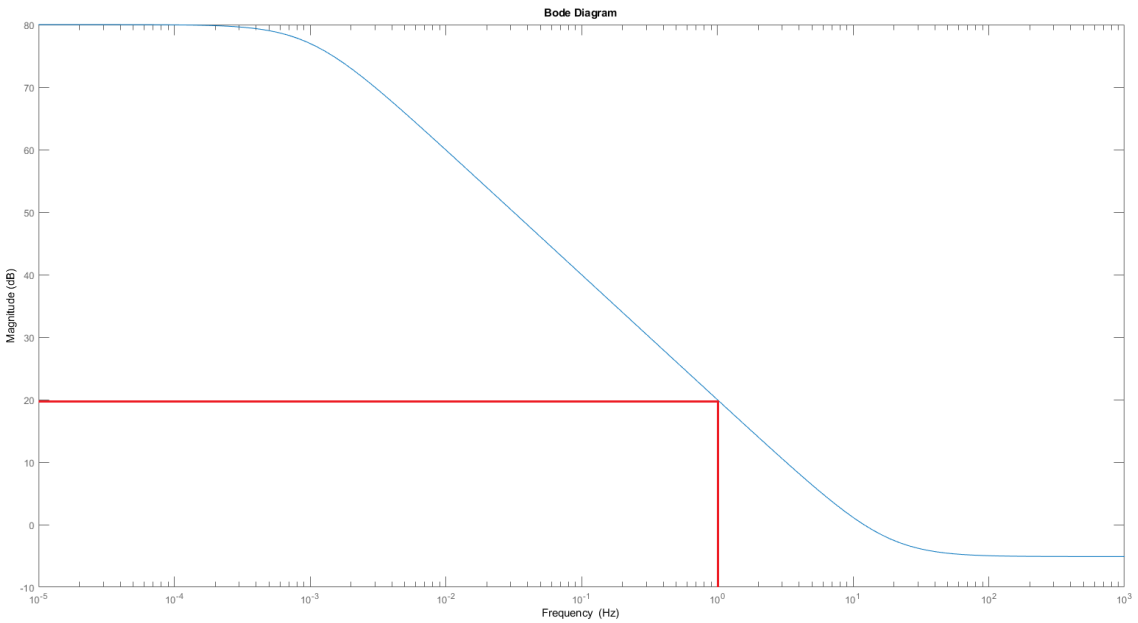

Figure 11: Designed weight W_p

3.3 Designing the control input weights

The requirement on the control input signal is to use the β input for lower frequency and the τ for higher frequency noise rejection. We saw from the RGA values in the previous part that close to the defined bandwidth frequency the τ torque has much more influence on the ω output than the β angle. Therefore, when designing the control input weight W_u we want to have high penalty in the transfer function from β to ω on higher frequencies. Regarding the transfer function from τ to ω we penalize the lower frequency components more. So similarly to W_p now we have:

$$|W_u KSG_d| < 1 \quad \rightarrow \quad |KSG_d| < W_u^{-1} \tag{29}$$

$$W_u = \begin{bmatrix} W_{u11} & 0 \\ 0 & W_{u22} \end{bmatrix} \tag{30}$$

Figure 12 shows the initial design for the weights. Since in the given input sequence the low frequency component is approximately in the order of $10^{-3}[Hz]$ the breakpoint for the bode plot of the W_{u11} weight is set to this frequency. For W_{u22} the breakpoint is set to be 2 decades higher, in order to have enough penalty around $10^{-3}[Hz]$.

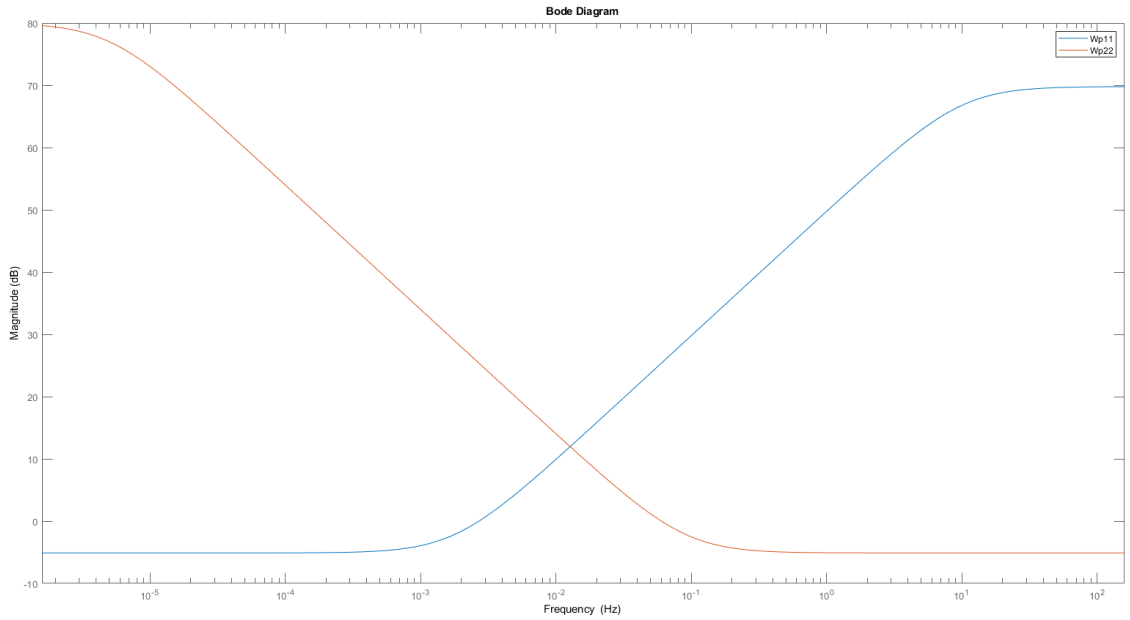

Figure 12: Initial design for the weights W_{u11} and W_{u22}

3.4 Iterative H_∞ controller design description

During the H_∞ controller synthesis the generalized plant is constructed using the robust control toolbox similarly to the previous part. The inverse of the weight will result in a not strict upper bound for the corresponding transfer function bode diagrams. With the designed controller it can be checked if the closed loop system validates these bounds or not. The γ value also gives an indication for that: if it is higher than 1, then these constraints are violated. At this point these constraint violations are not a problem if the achieved results are promising.

For the iterative controller design we also run the time-domain simulations using the given disturbance data.

For the initial design the transfer function Bode diagrams are plotted with their corresponding weight inverses. On Figure 13 it can be seen that although the limit is violated the design output error transfer function is nicely under $-20[dB]$ (even under $-30[dB]$). Figure 14 shows that we are penalizing the β control action for lower frequencies too much and that the τ input is acting also on lower frequencies.

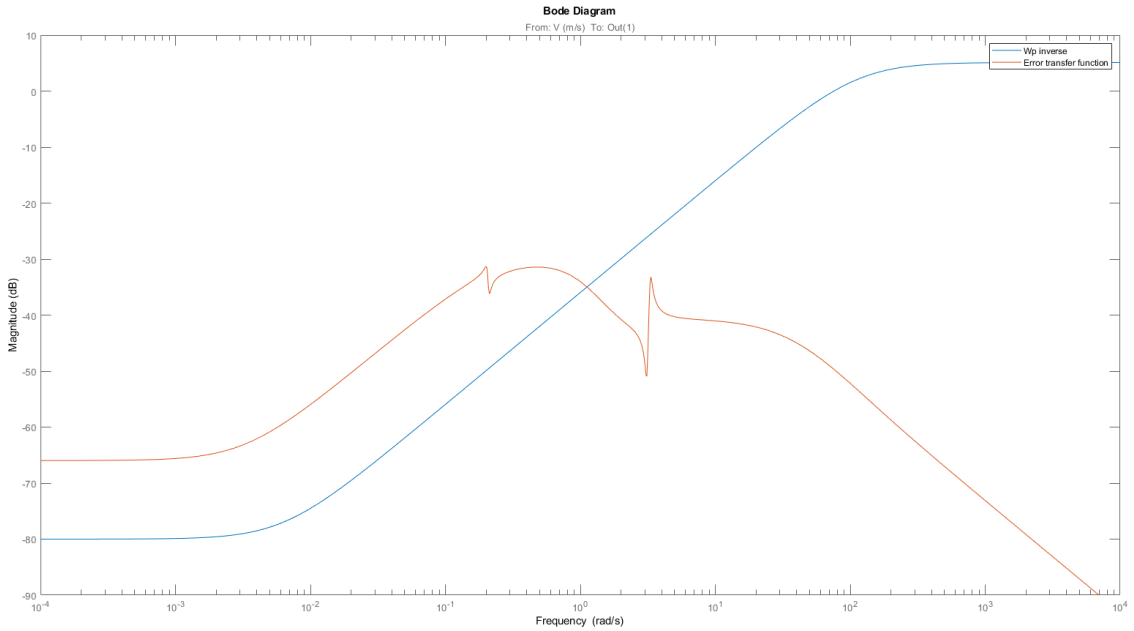

Figure 13: W_p inverse and SG_d (initial design)

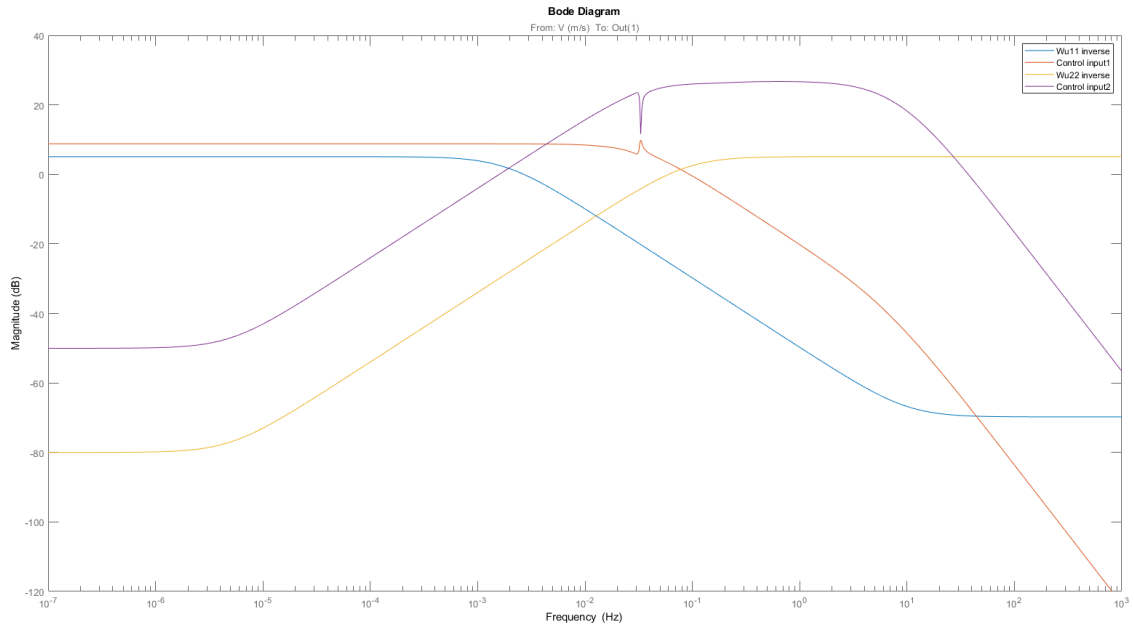

Figure 14: W_u inverse and KSG_d (initial design)

During the iterative design we modified the the weights according to the following general guidelines:

- Penalizing more the higher frequency components for the β transfer function if it had relatively high value there
- Penalizing more the lower frequency components for the τ transfer function if it also had relatively high value there
- Keeping the error transfer function bellow $-20[dB]$
- Decreasing the weight for the inputs on frequencies we want them to operate (for example letting β have even higher influence on low frequencies)

3.5 Final design validation, simulations

The controller design is validated by time-domain simulations, by applying different disturbance inputs to check the actuated control inputs and the error on the output.

3.5.1 Simulation with the real-life data

The simulation results are shown on Figure 16-18. The disturbance is nicely suppressed in the output (Figure 16). The β control counteracts mainly the low frequency components but it still acts somewhat also on higher frequencies as shown on Figure 17. This probably could be improved by further iterations in the controller design step. The rapid change in the τ torque input indicates that it counteracts the higher frequency components as desired.

One particular problem during the simulation was that the measured signal is not evenly spaced on the time axis and the MATLAB 'lsim' command expects an evenly spaced time vector. We therefore created an adequately dense time vector and interpolated the measured signal to that.

The next part contains further analysis on the operational frequency of the control input signals. There an artificially generated noiseless signal is used.

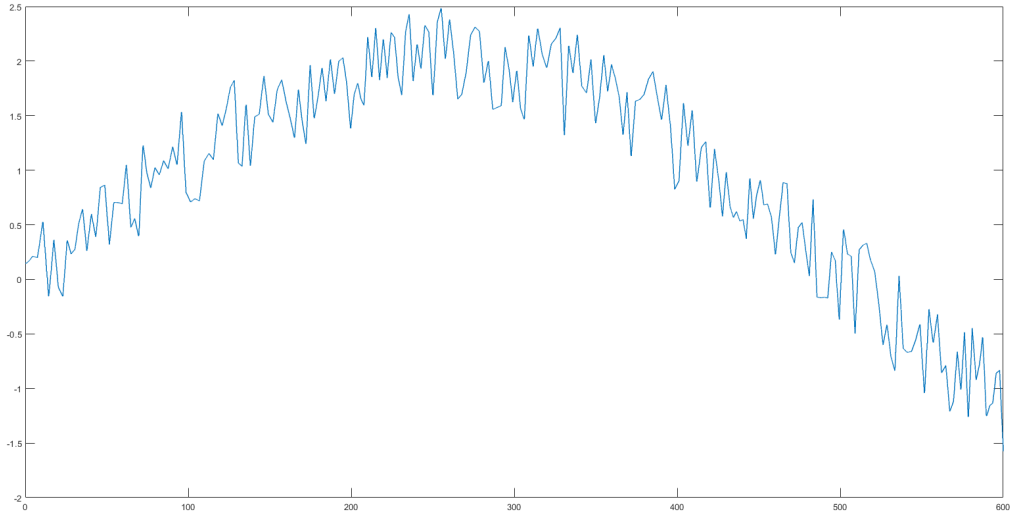

Figure 15: The given real-life disturbance input data

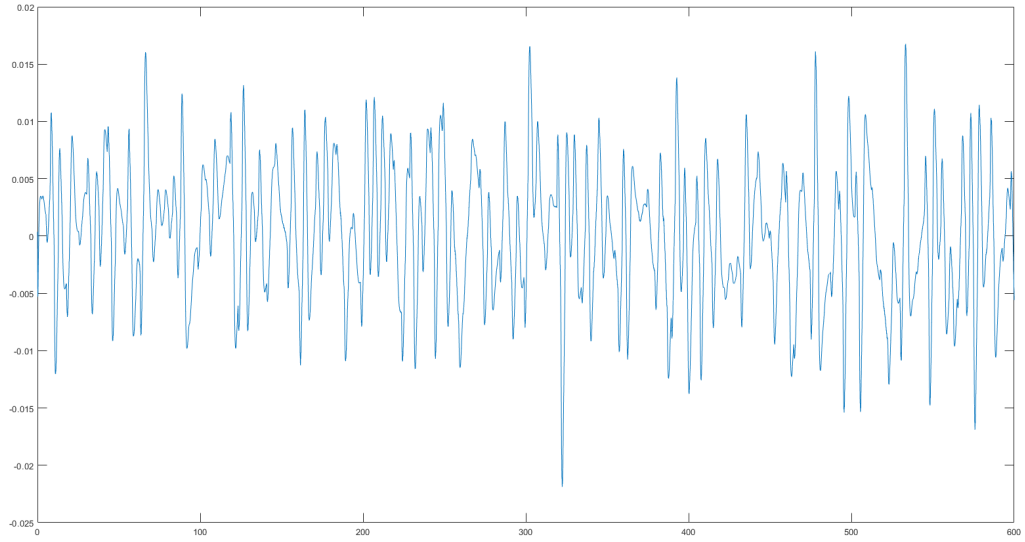

Figure 16: Simulated ω for the applied disturbance (real-life data)

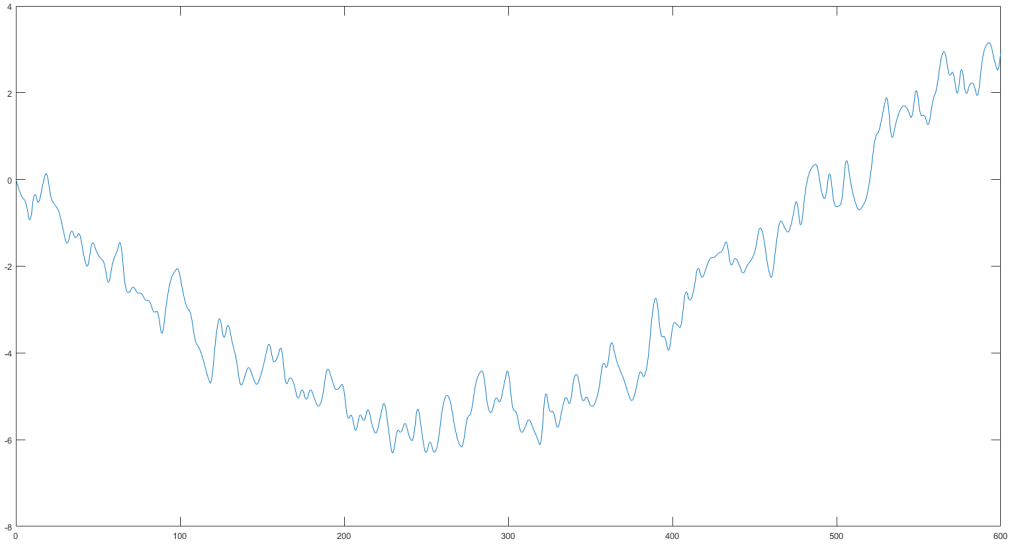

Figure 17: Simulated β control input (real-life data)

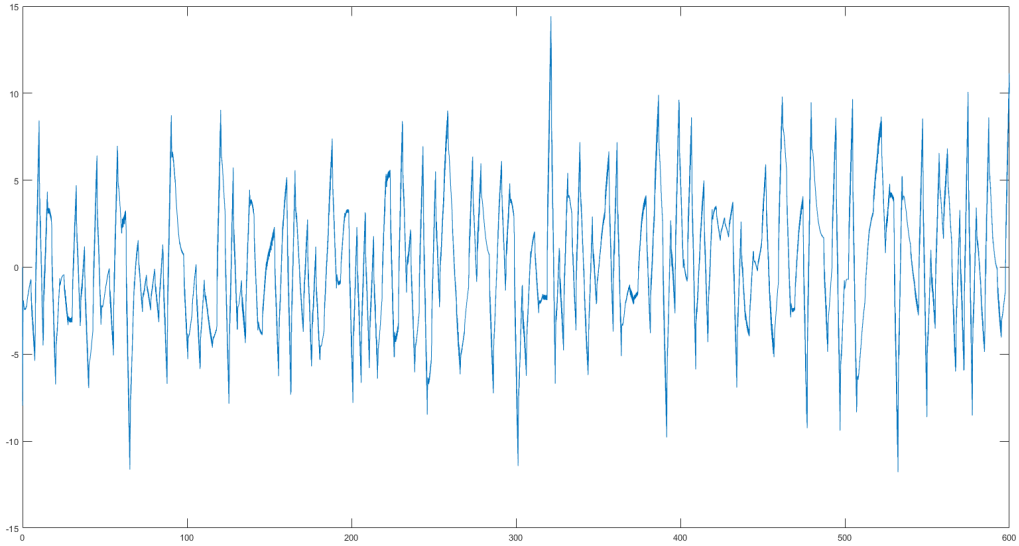

Figure 18: Simulated τ control input (real-life data)

3.5.2 Simulation with low frequency disturbance

In this part we simulated the system behaviour with a low frequency disturbance signal which has a similar amplitude and frequency as the low frequency component of the real-life data. The goal is to show that this kind of disturbance is mainly counteracted by the β input. So we expected small control action from the τ torque.

The "noiseless" signal is generated by looking at certain properties of the real-life data. The amplitude of the low frequency component is about $2[m/s]$. In the measurement there is a bit more than half a cycle completed by that signal. We read off from the diagram that half a cycle takes approximately $500[s]$, so a whole period would take $1000[s]$. The formula to generate the discrete-time low frequency signal:

$$d(k \cdot dt) = 2 \cdot sin(k \cdot dt \cdot 2\pi/1000) \tag{31}$$

, where d denotes the disturbance signal, k the index of the current time step and dt is the time step length.

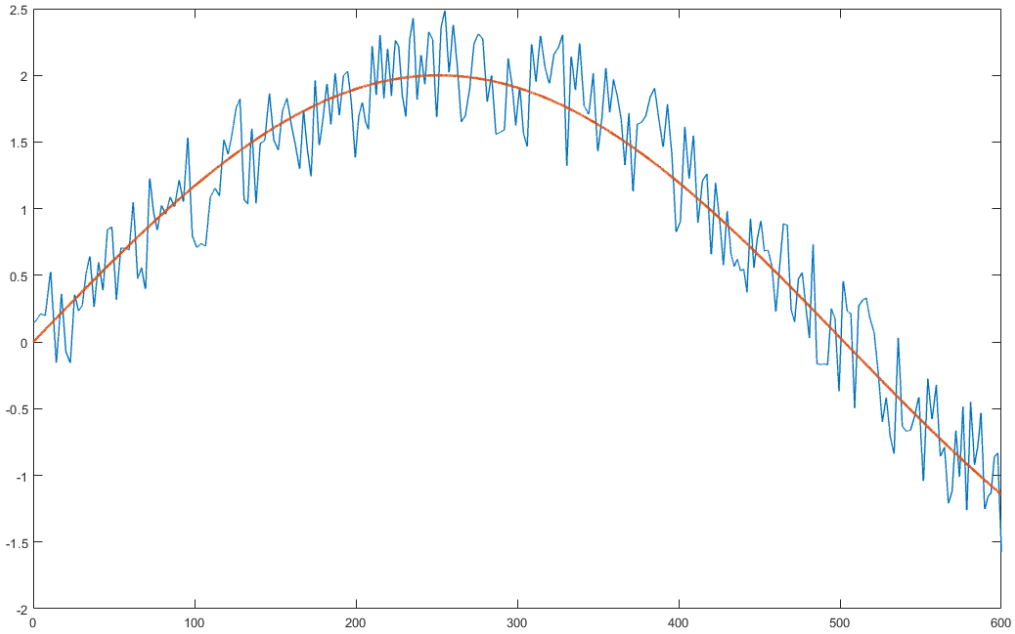

Figure 19: Approximation of the noiseless high amplitude component

Figure 20 shows the system output ω. The blue line shows the simulated signal from the previous simulation and the red one the low frequency disturbance response. It can be concluded that the controller eliminates the lower frequency components more effectively.

Figure 21-22 show how the control inputs are evolving over time. From these two figures it can be concluded that the β pitch angle is the one that counteracts the low frequency components mainly, because the τ torque input has small amplitude in this case.

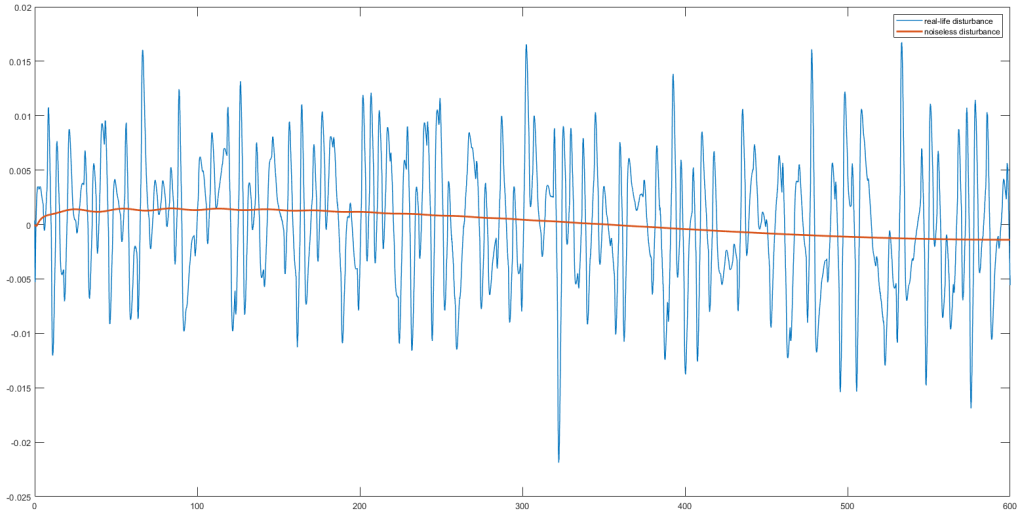

Figure 20: Simulated ω for the applied disturbance (low frequency disturbance)

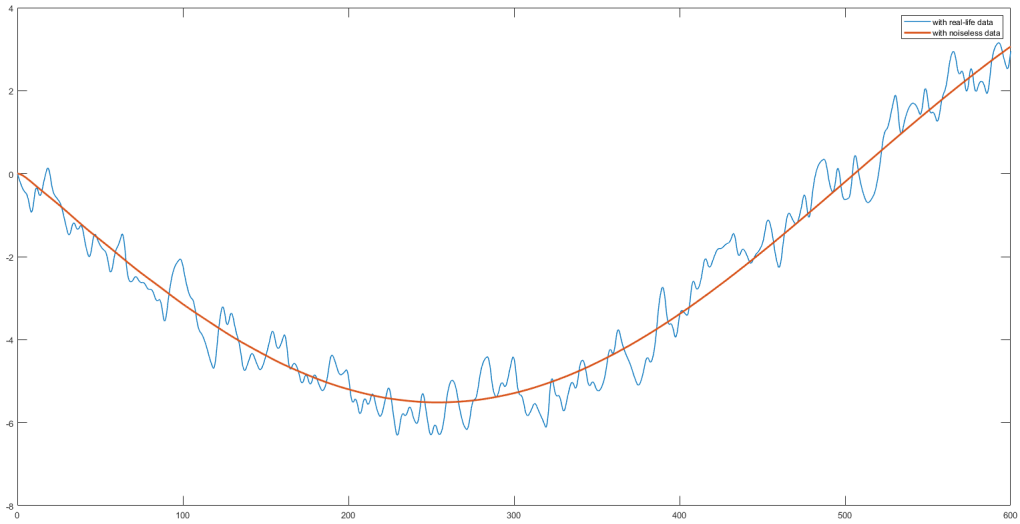

Figure 21: Simulated β control input (low frequency disturbance)

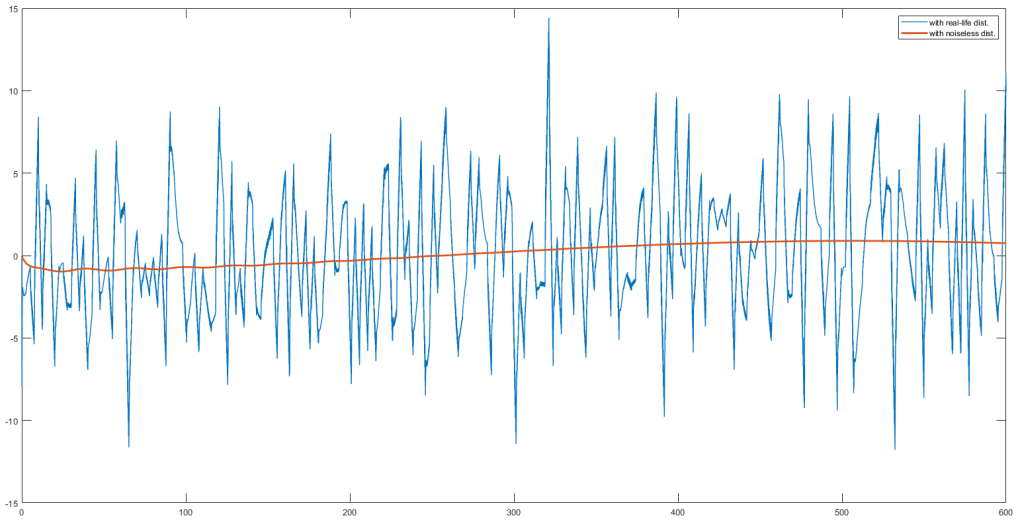

Figure 22: Simulated τ control input (low frequency disturbance)

References

[1] Sigurd Skogestad and I Postlethwaite. “Multivariable Feedback Control: Analysis and Design”. In: vol. 2. Jan. 2005.